

Quantifying diet-induced metabolic changes of the human gut microbiome

Saeed Shoaie¹, Pouyan Ghaffari¹, Petia Kovatcheva-Datchary², Adil Mardinoglu¹, Partho Sen¹, Estelle Pujos-Guillot³, Tomas de Wouters⁴, Catherine Juste⁴, Salwa Rizkalla^{5,6}, Julien Chilloux⁷, Lesley Hoyles⁷, Jeremy K. Nicholson⁷, ANR MicroObese Consortium, Joel Dore⁴, Marc E. Dumas⁷, Karine Clement^{5,6,8}, Fredrik Bäckhed^{2,9}, Jens Nielsen^{1*}

¹Department of Biology and Biological Engineering, Chalmers University of Technology, Kemivägen 10, SE-412 96 Gothenburg, Sweden

²Wallenberg Laboratory, Department of Molecular and Clinical Medicine and Sahlgrenska Center for Cardiovascular and Metabolic Research, University of Gothenburg, 413 45 Gothenburg, Sweden

³Institut National de la Recherche Agronomique, Nutrition Humaine, Plateforme Exploration du Métabolisme, F-63000 Clermont-Ferrand, France

⁴Institut National de la Recherche Agronomique, INRA, UMR1319 Micalis and USR 1367 MetaGenoPolis, Jouy-en-Josas, France

⁵Institute of Cardiometabolism and Nutrition, ICAN, Assistance Publique hôpitaux de Paris, Pitié-Salpêtrière hospital, 75013 Paris, France

⁶Institut National de la Santé et de la Recherche Médicale, INSERM, U1166, NutriOmics team 6, 75013 Paris, France

⁷Section of Biomolecular Medicine, Division of Computational and Systems Medicine, Department of Surgery and Cancer, Faculty of Medicine, Imperial College London, Exhibition Road, South Kensington, London SW7 2AZ, UK

⁸Sorbonne Universités, UPMC University Paris 06, UMR S-1166, Team 6, 75013 Paris, France

⁹Novo Nordisk Foundation Center for Basic Metabolic Research, Section for Metabolic Receptology and Enteroendocrinology, Faculty of Health Sciences, University of Copenhagen, 2200 Copenhagen, Denmark

Equally contributed

* Corresponding author

E-mail: nielsenj@chalmers.se

Tel: +46 31 772 3804

Fax: +46 31 772 3801

Running title: Metabolic modeling of the human gut microbiome

Summary

The human gut microbiome is known to be associated with various human disorders, but a major challenge is to go beyond association studies and elucidate causalities. Mathematical modeling of the human gut microbiome at a genome-scale is a useful tool to decipher microbe-microbe, diet-microbe and microbe-host interactions. Here, we describe the CASINO (Community and Systems-level Interactive Optimization) toolbox, a comprehensive computational platform for analysis of microbial communities through metabolic modeling. We first validated the toolbox by simulating and testing the performance of single bacteria and whole communities in *in vitro*. Focusing on metabolic interactions between the diet, gut microbiota and host metabolism, we demonstrated the predictive power of the toolbox in a diet-intervention study of 45 obese and overweight individuals, and validated our predictions by fecal and blood metabolomics data. Thus, modeling could quantitatively describe altered fecal and serum amino acid levels in response to diet intervention.

Introduction

Increasing evidence indicates that changes in the composition of the human gut microbiota affect host metabolism and are associated with a variety of diseases (Backhed et al., 2005; Qin et al., 2014). Changes in diet have been shown to rapidly affect the composition of the gut microbiota (David et al., 2014; Wu et al., 2011). Furthermore, microbiota-diet interactions impact host physiology through the generation of a number of bioactive metabolites (Cotillard et al., 2013; Le Chatelier et al., 2013; Nicholson et al., 2012; Wu et al., 2014). For example, short-chain fatty acids (SCFAs), which are generated by microbial fermentation of dietary polysaccharides in the gut, are an important energy source for colonocytes and also function as signaling molecules, modulating intestinal inflammation and metabolism (Donohoe et al., 2011; Fernandes et al., 2014; Samuel et al., 2008; Smith et al., 2013b; Tolhurst et al., 2012). In addition, dietary proteins and amino acids are important substrates for microbial fermentation in the colon (Cummings and Macfarlane, 1997) where they also serve as an important nitrogen source for the microbiota and support the growth of the microbiota and the host (Wu, 2009).

By quantifying the release and consumption of metabolites by the gut microbiota, it may be possible to elucidate interactions between the gut microbiota and host metabolism (Tremaroli and Backhed, 2012). This information would allow identification of diagnostic biomarkers and may provide insight into the role of the gut microbiota in disease progression (Karlsson et al., 2013; Qin et al., 2014; Zeller et al., 2014). A predictive systems-level model of the human gut microbiome is required to elucidate causalities and quantify the interactions between microbes, host and diet (Greenblum et al., 2013; Manor et al., 2014; Shoaie and Nielsen, 2014).

A genome-scale metabolic model (GEM) is an integrative platform for exploring genotype-phenotype relationships and metabolic differences between different clinical conditions (Ghaffari et al., 2015; Henry et al., 2010; Mardinoglu et al., 2014; Mardinoglu and Nielsen, 2015; Monk et al., 2014; Shoaie and Nielsen, 2014). We previously reconstructed GEMs to study the interactions between *Bacteroides thetaiotaomicron* and *Eubacterium rectale* (Shoaie et al., 2013),

representatives of Bacteroidetes and Firmicutes, the two dominant phyla in the human gut (Huttenhower et al., 2012), and between *Bifidobacterium adolescentis* and *Faecalibacterium prausnitzii* (El-Semman et al., 2014), also dominant and dietary-responsive gut microorganisms (Walker et al., 2011). In both studies, we manually identified the interactions between the bacteria and quantified the consumption and production rates of the defined interacting metabolites for each bacterial species. Although other studies have been conducted for communities of two and three species (Harcombe et al., 2014; Zomorodi and Maranas, 2012), these approaches cannot be expanded to simulate the interactions of a large number of species representing the complex gut ecosystem. We therefore developed the CASINO (Community And Systems-level Interactive Optimization) toolbox, which comprises an optimization algorithm integrated with diet analysis to predict the phenotypes and related dietary intake within the human gut microbiota. The toolbox was tested using both data from *in vitro* experiments and results from a nutritional intervention study of subjects with varying gut microbial gene richness.

Results

CASINO toolbox

We first developed an optimization algorithm in the CASINO toolbox, which is based on a collaborative and a multi-dimensional distributed approach (Grimm et al., 2005). It takes into account both collaboration between the multiple species as well as the fact that each individual species seeks to optimize its growth individually. Although GEMs are linear models, the presence of several GEMs in the overall community model means that the optimization of community biomass production becomes a non-linear problem. We therefore separated the community model into systems-level (representing the community) and organism-level (representing each species), which allowed us to linearize the optimization problem.

Simulations using CASINO start with an initialization stage that defines a primary profile of the systems-level topology (i.e. which species are present and how do they interact). This leads to the construction of a community matrix that defines effectors and receptors, with effectors being species that produce metabolites and receptors being species that consume metabolites. Following definition of the topology, the initialization step calculates metabolite production by each species using organism-level optimization. Thereafter, CASINO performs iterative multi-level optimization to calculate the relative uptake of carbohydrates by each species, until the total community biomass production is optimized. In this study, this calculation is constrained by the relative abundance of each species (**Experimental Procedures & Figure S1**).

To evaluate CASINO, we used the RAVEN toolbox (Agren et al., 2013) to update and significantly expand the content of our previously published GEMs for *B. thetaiotaomicron*, *E. rectale*, *B. adolescentis* and *F. prausnitzii* and to generate a GEM for *Ruminococcus bromii*, a representative of Clostridiales and a key gut symbiont (Ze et al., 2012). All GEMs were manually curated for functionality based on literature information. We defined a set of metabolic tasks, e.g. generation of biomass precursors (**Table S1**), to further investigate the functionality of the GEMs and checked that the resulting models could perform the defined tasks (**Experimental Procedures**).

The GEMs were functionally validated using experimental data for each of the five bacteria. We quantified the abundance of the bacteria by 16S ribosomal RNA (rRNA) quantitative PCR (qPCR) at baseline and after 24 h of growth in selected media (**Table S2; Extended Experimental Procedures**). We performed targeted metabolomics to quantify products of the fermentative activity of the studied bacteria, specifically the SCFAs butyrate, acetate and propionate and 15 different amino acids, and consumption of carbohydrates (glucose, maltose, cellobiose and starch). Flux constraints were imposed using the metabolomics profiles of the growth media, and maximum growth of each bacterial species was set as an objective function to simulate the predictive power of the corresponding model (**Experimental Procedures and Figure 1A**). The experimental data confirmed that the GEMs predicted the metabolism and biomass growth for each bacterial species almost perfectly (**Figures 1B-1D**). The GEMs correctly predicted that acetate can be produced by *B. adolescentis*, *B. thetaiotaomicron* and *R. bromii*, butyrate can be produced by *E. rectale* and *F. prausnitzii* and propionate can only be produced by *B. thetaiotaomicron* (**Figure 1B**). Our simulations also predicted that these five bacteria synthesize significantly higher level of essential amino acids (valine, leucine,

methionine, lysine and phenylalanine) compared to non-essential amino acids (serine, tyrosine and threonine) (**Figure 1D**).

Revealing the interactions between constituents of *in-vitro* microbial communities

To test the performance of CASINO, we simulated the interactions between the microbes in two microbial communities that differed only in one bacterial species: EBBR (*E. rectale*, *B. adolescentis*, *B. thetaiotaomicron* and *R. bromii*) and FBBR (*F. prausnitzii*, *B. adolescentis*, *B. thetaiotaomicron* and *R. bromii*) (**Figure 2A**). The simulated values were validated by culturing EBBR and FBBR communities in selected media. We quantified the abundance of individual bacterial species in each community by 16S rRNA-based qPCR (**Table S3**). We also performed targeted metabolomics to quantify the production of SCFAs and amino acids and the consumption of carbohydrates (starch and cellobiose) for each community (**Extended Experimental Procedures**).

Our model simulations correctly predicted the net production of the metabolites produced by each community and showed that the communities synthesized more essential amino acids than non-essential amino acids (**Figure 2B**). More importantly, the simulations enabled quantification of the contribution of each individual bacterial species to the overall microbial conversion in the communities and showed that two of the species in each community dominated. Specifically, we predicted that *B. thetaiotaomicron* and *E. rectale* synthesized 41% and 36% of the amino acids in the EBBR community, respectively, and *B. thetaiotaomicron* and *F. prausnitzii* synthesized 39% and 47% of the amino acids in the FBBR community, respectively (**Figure S2**). We also predicted that *E. rectale* mainly contributed to the synthesis of valine, leucine, phenylalanine and methionine in the EBBR community, while *F. prausnitzii* was the major contributor to the production of valine and leucine in the FBBR community. Furthermore, the experimental data showed that substitution of *E. rectale* with *F. prausnitzii* decreased the level of butyrate in the media, due to the higher capacity of *E. rectale* for butyrate production (Louis et al., 2010), and also the model simulations showed a slightly lower butyrate production by the FBBR community compared with the EBBR community.

Next we calculated the centrality scores for each bacterial species in order to identify which species have a dominant role in the overall metabolic conversion in each community (**Extended Experimental Procedures**). We observed that *E. rectale* and *B. thetaiotaomicron* were the main receptor and effector, respectively and thus represent key species (**Figure 3A**). We then evaluated the sensitivity of the optimization algorithm in CASINO by adding bacteria in three steps to each of these two bacteria, culminating in reconstruction of the two *in vitro* communities. We calculated the SCFA levels for each step (**Figure 3B**). Addition of *B. adolescentis* to *E. rectale* in the EBBR community resulted in reduced production of butyrate and increased production of propionate and acetate. Addition of *F. prausnitzii* to *B. thetaiotaomicron* in the FBBR community resulted in reduced production of propionate and acetate and increased butyrate production. The levels of the SCFAs changed further when the other species were added (**Figure 3B**).

Analyzing the effect of gene richness and diet on gut microbiota composition

To further evaluate CASINO, we examined data from a clinical study where 45 overweight and obese individuals were subjected to an energy-restricted high-protein diet with low glycemic index for 6 weeks (**Figure 4A**; clinical data in **Table S4**). These patients had previously been

stratified based on their gut microbial gene richness into ‘low gene count’ (LGC; n = 18) and ‘high gene count’ (HGC; n = 27) based on a cut-off threshold of 480,000 genes (Cotillard et al., 2013). LGC demonstrated a worse metabolic profile compared with HGC individuals (Cotillard et al., 2013).

Analysis of metagenomics data before and after the diet intervention showed that six species dominated in all subjects: *Escherichia coli* and *F. prausnitzii* and four species associated with Clostridia, Bacteroides, Bifidobacteria, and Lactobacillus (Cotillard et al., 2013). To obtain quantitative data of these species, we analyzed fecal samples by 16S rRNA qPCR before and after the dietary intervention (**Table S5 and Extended Experimental Procedures**) and used these results to calculate the distribution of biomass between the species (**Figure 4B**). We observed significant differences in abundance for *B. adolescentis*, *F. prausnitzii* and *E. rectale* at baseline and for *B. adolescentis* and *L. reuteri* after 6 weeks between LGC and HGC individuals. In HGC individuals, levels of *B. thetaiotaomicron* significantly increased and *L. reuteri* and *F. prausnitzii* significantly decreased after 6 weeks of dietary intervention compared with baseline, whereas a significant decrease in LGC individuals was only seen for *L. reuteri*.

Diet interventions alter amino acid and SCFA levels in HGC and LGC individuals

In order to simulate the effect of the diet on the overall gut microbiota metabolism, we used representatives of the most abundant microbial groups that we had also modeled *in vitro*, i.e. *B. thetaiotaomicron*, *B. adolescentis*, *F. prausnitzii*, *E. rectale* as described above and *Lactobacillus reuteri*, for which we reconstructed a GEM. We also performed simulations with inclusion of *E. coli*, but as this species had no major impact on the production of SCFAs and amino acids (data not shown), we did not include this species in our further analysis. Using CASINO, we simulated the effect of diet on the human gut microbiota composition at baseline and after the dietary intervention for 44 of the subjects (registered diet information in **Table S6**). In order to translate the diets into metabolites that can be utilized by the five gut bacterial species, we computed the dietary macronutrients of 24 different food items (**Table S7**) and used this information in a diet allocation algorithm in CASINO. Using this algorithm, CASINO predicted that there was a decrease in carbohydrate consumption and an increase in amino acid consumption for all individuals after 6 weeks of dietary intervention (**Figure 4C**). The intake of fiber from bread and potatoes, and to lesser extent rice, cereals and snacks, was decreased but fiber from fruits and vegetables was increased in agreement with the dietary recommendation given to the patient during the intervention (**Figure 4C**).

For the simulations, we assumed that carbohydrates and fibers were hydrolyzed to glucose to the same degree in all subjects, allowing us to calculate the relative amount of glucose available to the gut microbiome in each subject. We further assumed that glucose was the limiting substrate for the gut microbiome. We first used CASINO to quantify the community interactions and the relative glucose uptake by the individual species. We used the calculated values of species abundance in this process. Thereafter, we used CASINO to repeat the simulations, but now allowing the individual species to consume amino acids in the same ratio as their glucose uptake. The amount of available amino acids was calculated from the diet composition using CASINO.

With this approach we could simulate the profile of three SCFAs and 14 amino acids produced by the gut ecosystem as well as the contribution of each microbial species to the overall metabolite production of the ecosystem at baseline and after 6 weeks of dietary intervention for

each individual. By plotting average profiles for all the subjects, we found that the levels of the SCFAs and amino acids produced by the gut microbiota were significantly decreased after dietary intervention when both LGC and HGC groups were combined (**Figure 5A**, decrease in the y-axis direction), but the greatest reductions were observed in LGC individuals (**Figure 5A**, increase in the x-axis direction).

In order to experimentally evaluate our predictions on altered metabolite production by the gut ecosystem, we performed metabolomics analysis of fecal samples obtained from the HGC and LGC individuals at baseline and after 6 weeks of dietary intervention. These data confirmed the many of the predicted simulations by CASINO, i.e. alanine, proline, glycine, serine, phenylalanine, and tyrosine all showed a decreased level in response to the diet intervention in both HGC and LGC subjects but, with a larger decrease in the LGC subjects (**Figure 5B**, shift down-wards right). To test the significance of these changes for each group of subjects and between the two time points we calculated p -values using a student t-test, and except for alanine these changes were significant for the different groups (**Figure 5C**). Measured serine levels were significantly higher in LGC than HGC individuals at baseline but not after 6 weeks of dietary intervention (**Figure 5B**), in agreement with the predicted results (**Figure 5A**). Also, measured phenylalanine levels were significantly higher in LGC individuals than in HGC individuals at baseline but lower in LGC individuals compared to HGC subjects after 6 weeks of dietary intervention, in agreement with predicted results.

In addition to predicting changes in some of the metabolites in response to dietary intervention, the model could also be used to predict the relative contribution of each bacterial species to production of specific metabolites, allowing us to quantitatively assess how a variation in the gut microbiome correlates with metabolite production. Thus, we predicted the contribution of each bacterial species to phenylalanine levels in the gut ecosystem and showed that 23% of the total phenylalanine is produced by *B. adolescentis* and 26% by *E. rectale* in HGC individuals at baseline while this contribution increased for *B. adolescentis* to 26% and decreased for *E. rectale* by 21% after 6 weeks of dietary intervention (**Figure S3**). For LGC individuals, the contribution of *E. rectale* to phenylalanine production was 29% at baseline and decreased to 15% after 6 weeks of dietary intervention (**Figure S3**).

Serum metabolomics confirm model predictions and associate with clinical parameters

Although the model simulations could correctly predict changes in several of the metabolites in the feces, we noted that the model simulations did not accurately predict changes in all the measured metabolites, which may be a result of differential absorption by the host. We therefore evaluated whether the model could predict changes in the serum. We used metabolomics to analyze serum of the 45 subjects at baseline and after 6 weeks of dietary intervention and found an excellent correspondence between the model predictions (**Figure 5A**) and the measured changes (**Figure 6A**). The serum levels of 10 detected amino acids decreased in response to the dietary intervention in the LGC subjects (**Figure 6A**). Furthermore, in agreement with the model predictions, there was a decrease in acetate in response to the diet intervention in all subjects (**Figure 6A**). In addition, we observed that phenylalanine levels were higher in LGC subjects compared to HGC subjects at baseline, but the level of phenylalanine decreased in LGC subjects after 6 weeks of dietary intervention (**Figure 6A and 6B**). We also observed that levels of valine, leucine and alanine were higher in LGC subjects at baseline (**Figure 6A and 6B**).

To evaluate if these changes in serum metabolite levels may have any clinical relevance, we analyzed the correlations between the levels of the 10 amino acids in the serum and bioclinical parameters of the subjects at baseline (**Figure 6C**). Here we found that the serum phenylalanine levels were positively correlated with clinical variables related to body corpulence (BMI, DXA-measure fat mass, waist circumference, leptin), insulin resistance, blood lipid homeostasis (serum triglycerides and cholesterol), and low-grade inflammation (hsCRP). The serum levels of valine, leucine were also positively correlated with BMI.

Model-based diet design to improve metabolism of LGC individuals

Finally, assuming that LGC subjects have a non-optimal gut microbiome metabolism (associated with a clinically altered metabolism) we wanted to identify which dietary change would improve the metabolism of their gut microbiome. We thus made the assumption that an adapted dietary recommendation in LGC subjects provided at baseline would enable them to reach the “optimal” gut microbiome metabolism of HGC subjects after 6 weeks of dietary intervention, which is indeed associated with an improved metabolic phenotype.

.We then used CASINO and the abundance of the five different species, *i.e.* *B. thetaiotaomicron*, *B. adolescentis*, *F. prausnitzii*, *E. rectale* and *L.reuteri*, to predict the relative consumption of 8 essential amino acids by the gut microbiome in the LGC subjects at baseline (base phenotype in **Figure 7A**) and in the HGC subjects at week 6 (improved phenotype in **Figure 7A**).

From this model analysis, we found that the gut microbiome of HGC individuals had a higher consumption of these 8 essential amino acids at week 6 compared to that of the LGC subjects at baseline. An incremental augmentation of these amino acids would permit to acquire a similar metabolism of the gut microbiome in LGC and HGC subjects (**Figure 7A**). Many different combinations of food sources could fulfill such a requirement for essential amino acids. However, in an attempt to identify some overall guidelines, we correlated the difference between the two different requirements of amino acids with the composition of these amino acids in different food types (**Table S8**). This showed that LGC individuals should significantly increase consumption of dairy products, vegetables, white meat, fish pulses, eggs, oils and butter. In the meantime, they should considerably reduce intake of pastries, bread and rice to improve and slightly reduce intake of cereals and nuts (**Figure 7B**).

Discussion

The overall metabolism of the gut microbiome can be modeled in one of two ways: 1) by using a lumped model of all the metabolic reactions active in the different gut microorganisms or 2) by compartmentalizing the metabolism according to the individual microorganisms. The latter is clearly a better reflection of the true biological system and it also ensures that redox and energy balances are constrained within each organism considered. We therefore used this approach to model the metabolism of the human microbiome and reconstructed GEMs for individual species from the predominant phyla in the human gut. We identified which species to include in our analysis based on their abundance in the gut ecosystem. Thus, we reconstructed GEMs for five species that are representative bacteria of the dominant phyla in the human gut and we hypothesized that the reactions included in our models cover most of the metabolic functions that are present in the human gut. Compared with earlier attempts to model the human gut metabolism using GEMs, *i.e.* the COMETS algorithm (Harcombe et al., 2014), CASINO allows inclusion of

several species in the simulations. Furthermore, it is scalable and enables expansion to include even more than the five species that we considered in this study.

In order to evaluate whether we are covering the main metabolic functions, we simulated the effect of different diets, studied the interactions between the microbes and host in response to the diet, and quantified the contribution of each bacterial species to the fecal metabolite profiling. The model simulations matched fecal metabolomics data, but more importantly it correctly correlated with changes in serum levels of 10 amino acids and one SCFA (acetate). Thus, the model captures some major metabolic functions of the human gut microbiome. In the future, the selection of species to be considered should be expanded, in particular to ensure representation of more specific metabolic functions such as vitamin biosynthesis and bile acid metabolism.

The consistency between model predictions of metabolite productions and measurement of changes in metabolite levels in feces and serum suggests that our modeling correctly predicts the overall carbon fluxes in the gut ecosystem. Furthermore, our simulations enabled quantification of how the individual species compete for nutrients and produce different metabolites that may serve as nutrients for other species or be absorbed by the host. Studying the gut metabolism with our holistic approach also enabled understanding of metabolic shifts under different clinical conditions, and hereby could provide a direct link between the gut microbiome metabolism and serum chemistry.

Thus, our simulations suggest that the gut microbiome may contribute to altered levels of several amino acids in the serum, including phenylalanine and branched chain amino acids. This is in line with an early report, using germ free mice, showing that the microbiota of the large intestine increased the free amino acid level in the gastrointestinal tract (Macfarlane et al., 1988). A later study showed that bacteria in the human large intestine take up peptides and amino acids, and convert these to different amino acids and SCFAs (Smith and Macfarlane, 1998). This study also showed that the production of amino acids was dependent on the composition of starch, proteins and peptides, and hence will be dependent on the dietary composition. Further confirmation of our findings is documented in a recent review on the role of microbial amino acid metabolism in host metabolism, that provide a summary on a number of findings related to the role of the microbiota in the large intestine on production of not only SCFAs but also amino acids that are subsequently taken up by the host (Neis et al., 2015). However, we are aware that more experiments are required to validate if the gut microbiome actually contribute to host amino acid metabolism.

In our study, obese individuals with a LGC microbiome, associated with more impaired metabolic phenotype compared with those with HGC, had elevated levels of these amino acids. A previous study has shown that phenylalanine is associated with type 2 diabetes (T2D), and serum levels of this essential amino acid are five to seven fold higher in individuals at risk of T2D compared to control subjects (Wang et al., 2011). Furthermore, the serum level of branched chain amino acids (valine, leucine and isoleucine) has been found to correlate with insulin resistance (Newgard et al., 2009). Circulating levels of leucine, arginine, valine, proline, phenylalanine, isoleucine and lysine are also significantly associated with an increased risk of hypertriglyceridemia in diabetic subjects (Mook-Kanamori et al., 2014), a phenotype we noted in the subjects with the LGC microbiome. Thus, our simulations point to two important findings. First it suggests that the gut microbiota in LGC individuals may contribute to increased serum levels of many amino acids that have been found correlated with metabolic diseases such as T2D,

and we believe this is consistent with the deteriorated glucose homeostasis related to insulin resistance observed for the LGC subjects at baseline both in French and Danish subjects (Cotillard et al., 2013; Le Chatelier et al., 2013). The HGC subjects on the other hand, with their more gene rich gut microbiome may have a better conversion of amino acids, resulting in lower levels of these in the plasma. Furthermore, the HGC microbiome also have higher capacity to produce SCFAs that are important energy sources for the colonocytes as well as they function as signaling molecules, modulating intestinal inflammation and metabolism (Donohoe et al., 2011; Fernandes et al., 2014; Samuel et al., 2008; Smith et al., 2013b; Tolhurst et al., 2012). Second, in agreement with the original study on the LGC in comparison to the HGC individuals, it highlights that LGC subjects can benefit from a dietary intervention that improve their gut microbiome metabolism, paving the way for a personalized approach in these subjects. Indeed, despite higher levels of some amino acids at baseline, LGC subjects had a larger decrease in the levels of a range of metabolites that are positively correlated with insulin resistance markers and cardio-metabolic risk factors.

Using our approach we also predicted the relative contribution of each bacterial species to production of specific metabolites, and studied how this variation in the gut microbiome is correlated with specific metabolite production. Information generated from CASINO may therefore be extended for rational design of prebiotics as well as for identifying novel beneficial bacteria that can be used to fortify the microbiota to improve the gut microbiome metabolism. Importantly, rational design of microbiota interventions requires knowledge of diet as demonstrated in a study of children with kwashiorkor which showed that a disrupted microbiome that can be reversed by dietary interventions (Smith et al., 2013a). Interestingly, transferring the microbiota from children with kwashiorkor to germ-free mice in combination with Malawian diet resulted in marked weight loss in recipient mice associated with perturbations in amino acids. As we demonstrated CASINO can also be used to predict dietary changes required in order to ensure a certain profile of the gut metabolism, here represented as a specific consumption of 8 essential amino acids. The gut microbiome may change in response to dietary modulation, something that our simulations are not capturing. This study also emphasizes the importance of developing accurate tools to properly record dietary intakes in different populations. With more data it will probably be possible to also predict how the diet influences gut microbiome changes, and hereby CASINO may assist in the development of a precision medicine approach to treat metabolic diseases associated with dysfunction of the gut microbiota.

In conclusion, we demonstrate how we can use model simulations to predict metabolic interactions within the gut microbiome and hereby assist in generating mechanistic insight into the contribution of individual species of the gut microbiome to the overall metabolism of the ecosystem and the host. Furthermore, focused on the diet and on host and gut microbiota metabolic interactions we show how the gut ecosystem and the individual members of the gut microbiota contribute to the host metabolism. CASINO may thus constitute a valuable tool for enriching the information content provided by gut metagenome analysis, and hereby advance our understanding on how this important metabolic organ contributes to disease development and thus facilitate personalized interventions based on the microbiome.

Experimental procedures

Reconstruction/updating of GEMs

The *B. adolescentis*, *B. thetaiotaomicron*, *E. rectale* and *F. Prausnitzii* metabolic models were already published (El-Semman et al., 2014; Shoaie et al., 2013). These models were validated individually and updated based on extensive bibliometric survey of the literature and databases (Henry et al., 2010). The *R. bromii* and *L. reuteri* metabolic networks were reconstructed based on automatic and manual curation, considering information available in the literature and databases. For model reconstructions, updating and quality checks, the RAVEN toolbox was used (Agren et al., 2013). The defined metabolic task file was implemented to perform the gap filling process. This task file includes synthesis of amino acids, nucleotides and carbohydrates. A published metabolic model for *E. coli* was used for simulation (Monk et al., 2013).

Validation of GEMs

The metabolic models for *B. adolescentis*, *B. thetaiotaomicron*, *E. rectale* and *F. prausnitzii* and *R. bromii* were used to predict the experimental phenotypes based on the individual *in-vitro* data. The growth for each model was predicted as an objective function based on the available media components from the experiments. Measured amino acids and SCFAs secretion were used to constrain the models for individual simulations. The lower and upper bounds for the uptake and secretion reactions were assigned based on standard deviation of the measured metabolites in experimental data. The results were tested to see the consistency of the model through fixation of non-growth associated maintenance ATP.

CASINO toolbox

CASINO defines the primary topology of the community and identifies optimum solution by applying a multi-dimensional optimization procedure in two successive and connected stages: Initialization and Community optimization. The convexity of the solution space and linearity of the parameters are maintained by separating the problem into two independent optimizing dimensions, systems-level and organism-level, with three classes of variables: inputs, outputs and connecting parameters. Maximum biomass production was considered as objective function at both levels. At the organism level, each species seeks to maximize its biomass yield while at the system level the community seeks to stay in optimum balanced condition by synchronizing the competition between species (**Figure S1**).

Initialization process assumes a structure of the community as a complex network and starts with an activation cascade supporting a specific threshold. Species are categorized into primary (grows independently by taking up system-level inputs) and non-primary (growth is dependent on connecting inputs, i.e. metabolites produced by other species) classes. The activation begins with identifying primary species within the community and activates them by providing required resources to grow. The compounds produced by activated species are added to the resource pool and the community is screened again to find non-primary species that now can grow based on the updated resource pool. This cascade of activation is repeated until the whole network has been activated. Now a feasible profile of community topology is constructed and this results in a definition of the community constraints matrix and the community objective function. At the end of the initialization process the system is locally optimum (species grow on maximum biomass

yield rate) but globally non-optimum (resources distribution between species do not satisfy community optimum conditions).

Community optimization, a multi-level iterative process, starts based on the initial feasible space and a community objective function defined by the initialization procedure. In each step, the community level biomass production is optimized to find the optimum distribution of resources between species. Relative carbohydrate uptake rates are calculated in each intermediate systems-level optimum condition and these are used by the species to reach organism-level optimality. Metabolites secretion rates obtained after organism-level optimization is used to expand the boundaries of the intermediate feasible space and find a new system-level optimum. This iterative process continues until the solution converges to local and global optima.

Objective function in this algorithm is considered as maximum biomass yield (local force) at the organism-level and maximum community biomass (community force) at the system-level. Summation of these two forces defines the direction of optimization through expansion of the feasible space. The community force is adjusted by centrality scores assigned to each species based on the network topology of the community established in the initialization procedure. Two centrality degrees, power centrality and degree centrality, are used to calculate controlling power of species as effectors and receptors.

$$\text{Maximize } S = [\varphi \times \theta']. C_E. \omega_{\mu}. \delta$$

Where

$$s = \alpha.X + \beta.Z^{in} + \gamma.Y + \delta.Z^{out}$$

$$\omega_{\mu} = \frac{\mu(i)}{\min(\mu_{PL})}$$

$$\begin{aligned} \varphi &= [\alpha, \beta, \gamma, \delta] : \text{Coefficients matrix} \\ \theta &= [X, Y, Z] : \text{Inputs, outputs and connecting parameters} \\ PL & : \text{Primary species list} \end{aligned}$$

δ is a binary vector that activates certain parameter in the objective equation. This binary vector is corrected by imposing the relative centrality scores of species. $\mu(i)$ is the biomass yield of individuals and μ_{PL} is biomass yield of species belong to PL.

Statistical Analysis

Peaks obtained from 144 samples (HGC and LGC subjects) at two different time points (0 hours and 6 weeks) was aligned and subjected to retention time correction, XCMS (Smith et al., 2006). About 295 features (mz) with aligned peak were normalized by Quantile normalization method (Amaratunga and Cabrera, 2001). Mass fragmentation spectra of each featured peak were matched against the reference spectra obtained from Metlin (Tautenhahn et al., 2012) and HMDB (Wishart et al., 2013) using exact template matching approach (Pavlidis, 2003). Spectra with 90% match probability were considered for further analysis. Again, the retention index of the matched peak(s) (mz) was verified with metabolites in HMDB (Wishart et al., 2013). Thus, spectral match and retention index ensure identification and annotation of metabolites. Intensity (or expression) of 15 metabolites of interest was extracted for HGC and LGC subjects at two time points. Two sample t-tests were performed for detecting the significant metabolites and P value < 0.05 was considered to be significant. All data are shown as mean \pm 1 SD.

Author contribution

JN conceived and designed the study. SS and PG developed the toolbox. SS and AM reconstructed and updated the GEMs. FB and PKD designed the *in vitro* experiments and PKD performed the *in-vitro* experiments, and analyzed the samples. KC designed the clinical study and coordinated sample analysis. JPF performed qPCR on fecal samples. KC and SR performed the clinical investigation. CJ and TW performed the fecal water extraction and EPG performed untargeted metabolomics on fecal samples. SS, PG, PKD and AM analyzed the data. PS performed *in-silico* analysis on untargeted metabolomics. JC, LH, ALN performed NMR, JC and MED assigned the NMR data, JC, LH JKN and MED analyzed the data. JN, FB, KC, AM and SS wrote the manuscript.

Competing financial interests

The authors declare no competing financial interests.

Acknowledgements

We thank Dr. Rosie Perkins (University of Gothenburg) for editing the manuscript, Dr Ana Luisa Neves for NMR sample preparation and Suwanee Jansa-Ard for metabolomics sample preparation. This project was supported by Knut and Alice Wallenberg Foundation, the Bill & Melinda Gates Foundation, Torsten Söderbergs Stiftelse, European Commission FP7 project METACARDIS with the grant agreement HEALTH-F4-2012-305312, Fondation Cœur et Artères and French National Agency of Research (ANR-MicroObese, and “Investissements d’avenir” ANR-10-IAHU-05).

ANR MicroObese consortium members

Verger E, Cotillard A, Kennedy SP, Prifti E, Pons N, Le Chatelier E, Almeida M, Quinquis B, Levenez F, Galleron N, Gougis S, Batto JM, Ehrlich D, Blottière H, Lepage P, Maguin E, Van de Guchte M, Zucker JD.

References

- Agren, R., Liu, L., Shoaie, S., Vongsangnak, W., Nookaew, I., and Nielsen, J. (2013). The RAVEN toolbox and its use for generating a genome-scale metabolic model for *Penicillium chrysogenum*. *PLoS computational biology* 9, e1002980.
- Amaratunga, D., and Cabrera, J. (2001). Analysis of data from viral DNA microchips. *J Am Stat Assoc* 96, 1161-1170.
- Backhed, F., Ley, R.E., Sonnenburg, J.L., Peterson, D.A., and Gordon, J.I. (2005). Host-bacterial mutualism in the human intestine. *Science* 307, 1915-1920.
- Cotillard, A., Kennedy, S.P., Kong, L.C., Prifti, E., Pons, N., Le Chatelier, E., Almeida, M., Quinquis, B., Levenez, F., Galleron, N., *et al.* (2013). Dietary intervention impact on gut microbial gene richness. *Nature* 500, 585-588.
- Cummings, J.H., and Macfarlane, G.T. (1997). Colonic microflora: nutrition and health. *Nutrition* 13, 476-478.
- David, L.A., Maurice, C.F., Carmody, R.N., Gootenberg, D.B., Button, J.E., Wolfe, B.E., Ling, A.V., Devlin, A.S., Varma, Y., Fischbach, M.A., *et al.* (2014). Diet rapidly and reproducibly alters the human gut microbiome. *Nature* 505, 559-563.
- Donohoe, D.R., Garge, N., Zhang, X., Sun, W., O'Connell, T.M., Bunger, M.K., and Bultman, S.J. (2011). The microbiome and butyrate regulate energy metabolism and autophagy in the mammalian colon. *Cell metabolism* 13, 517-526.
- El-Semman, I.E., Karlsson, F.H., Shoaie, S., Nookaew, I., Soliman, T.H., and Nielsen, J. (2014). Genome-scale metabolic reconstructions of *Bifidobacterium adolescentis* L2-32 and *Faecalibacterium prausnitzii* A2-165 and their interaction. *BMC systems biology* 8, 41.
- Fernandes, J., Su, W., Rahat-Rozenbloom, S., Wolever, T.M., and Comelli, E.M. (2014). Adiposity, gut microbiota and faecal short chain fatty acids are linked in adult humans. *Nutrition & diabetes* 4, e121.
- Ghaffari, P., Mardinoglu, A., Asplund, A., Shoaie, S., Kampf, C., Uhlen, M., and Nielsen, J. (2015). Identifying anti-growth factors for human cancer cell lines through genome-scale metabolic modeling. *Sci Rep* 5, 8183.
- Greenblum, S., Chiu, H.C., Levy, R., Carr, R., and Borenstein, E. (2013). Towards a predictive systems-level model of the human microbiome: progress, challenges, and opportunities. *Current opinion in biotechnology* 24, 810-820.
- Grimm, V., Revilla, E., Berger, U., Jeltsch, F., Mooij, W.M., Railsback, S.F., Thulke, H.H., Weiner, J., Wiegand, T., and DeAngelis, D.L. (2005). Pattern-oriented modeling of agent-based complex systems: lessons from ecology. *Science* 310, 987-991.
- Harcombe, W.R., Riehl, W.J., Dukovski, I., Granger, B.R., Betts, A., Lang, A.H., Bonilla, G., Kar, A., Leiby, N., Mehta, P., *et al.* (2014). Metabolic resource allocation in individual microbes determines ecosystem interactions and spatial dynamics. *Cell reports* 7, 1104-1115.
- Henry, C.S., DeJongh, M., Best, A.A., Frybarger, P.M., Linsay, B., and Stevens, R.L. (2010). High-throughput generation, optimization and analysis of genome-scale metabolic models. *Nature biotechnology* 28, 977-982.
- Huttenhower, C., Gevers, D., Knight, R., Abubucker, S., Badger, J.H., Chinwalla, A.T., Creasy, H.H., Earl, A.M., FitzGerald, M.G., Fulton, R.S., *et al.* (2012). Structure, function and diversity of the healthy human microbiome. *Nature* 486, 207-214.
- Karlsson, F.H., Tremaroli, V., Nookaew, I., Bergstrom, G., Behre, C.J., Fagerberg, B., Nielsen, J., and Backhed, F. (2013). Gut metagenome in European women with normal, impaired and diabetic glucose control. *Nature* 498, 99-103.

Le Chatelier, E., Nielsen, T., Qin, J., Prifti, E., Hildebrand, F., Falony, G., Almeida, M., Arumugam, M., Batto, J.M., Kennedy, S., *et al.* (2013). Richness of human gut microbiome correlates with metabolic markers. *Nature* 500, 541-546.

Louis, P., Young, P., Holtrop, G., and Flint, H.J. (2010). Diversity of human colonic butyrate-producing bacteria revealed by analysis of the butyryl-CoA:acetate CoA-transferase gene. *Environmental microbiology* 12, 304-314.

Macfarlane, G.T., Allison, C., Gibson, S.A., and Cummings, J.H. (1988). Contribution of the microflora to proteolysis in the human large intestine. *The Journal of applied bacteriology* 64, 37-46.

Manor, O., Levy, R., and Borenstein, E. (2014). Mapping the Inner Workings of the Microbiome: Genomic- and Metagenomic-Based Study of Metabolism and Metabolic Interactions in the Human Microbiome. *Cell metabolism* 20, 742-752.

Mardinoglu, A., Agren, R., Kampf, C., Asplund, A., Uhlen, M., and Nielsen, J. (2014). Genome-scale metabolic modelling of hepatocytes reveals serine deficiency in patients with non-alcoholic fatty liver disease. *Nat Commun* 5, 3083.

Mardinoglu, A., and Nielsen, J. (2015). New paradigms for metabolic modeling of human cells. *Current opinion in biotechnology* 34C, 91-97.

Monk, J., Nogales, J., and Palsson, B.O. (2014). Optimizing genome-scale network reconstructions. *Nature biotechnology* 32, 447-452.

Monk, J.M., Charusanti, P., Aziz, R.K., Lerman, J.A., Premyodhin, N., Orth, J.D., Feist, A.M., and Palsson, B.O. (2013). Genome-scale metabolic reconstructions of multiple *Escherichia coli* strains highlight strain-specific adaptations to nutritional environments. *Proceedings of the National Academy of Sciences of the United States of America* 110, 20338-20343.

Neis, E.P.J.G., Dejong, C.H.C., and Rensen, S.S. (2015). The Role of Microbial Amino Acid Metabolism in Host Metabolism. *Nutrients* 7, 2930-2946.

Newgard, C.B., An, J., Bain, J.R., Muehlbauer, M.J., Stevens, R.D., Lien, L.F., Haqq, A.M., Shah, S.H., Arlotto, M., Slentz, C.A., *et al.* (2009). A branched-chain amino acid-related metabolic signature that differentiates obese and lean humans and contributes to insulin resistance. *Cell metabolism* 9, 311-326.

Nicholson, J.K., Holmes, E., Kinross, J., Burcelin, R., Gibson, G., Jia, W., and Pettersson, S. (2012). Host-gut microbiota metabolic interactions. *Science* 336, 1262-1267.

Pavlidis, P. (2003). Using ANOVA for gene selection from microarray studies of the nervous system. *Methods* 31, 282-289.

Qin, N., Yang, F., Li, A., Prifti, E., Chen, Y., Shao, L., Guo, J., Le Chatelier, E., Yao, J., Wu, L., *et al.* (2014). Alterations of the human gut microbiome in liver cirrhosis. *Nature* 513, 59-64.

Samuel, B.S., Shaito, A., Motoike, T., Rey, F.E., Backhed, F., Manchester, J.K., Hammer, R.E., Williams, S.C., Crowley, J., Yanagisawa, M., *et al.* (2008). Effects of the gut microbiota on host adiposity are modulated by the short-chain fatty-acid binding G protein-coupled receptor, Gpr41. *Proceedings of the National Academy of Sciences of the United States of America* 105, 16767-16772.

Shoaie, S., Karlsson, F., Mardinoglu, A., Nookaew, I., Bordel, S., and Nielsen, J. (2013). Understanding the interactions between bacteria in the human gut through metabolic modeling. *Sci Rep* 3, 2532.

Shoaie, S., and Nielsen, J. (2014). Elucidating the interactions between the human gut microbiota and its host through metabolic modeling. *Frontiers in Genetics* 5, 86.

Smith, C.A., Want, E.J., O'Maille, G., Abagyan, R., and Siuzdak, G. (2006). XCMS: Processing mass spectrometry data for metabolite profiling using Nonlinear peak alignment, matching, and identification. *Anal Chem* *78*, 779-787.

Smith, E.A., and Macfarlane, G.T. (1998). Enumeration of amino acid fermenting bacteria in the human large intestine: effects of pH and starch on peptide metabolism and dissimilation of amino acids. *FEMS Microbiology Ecology* *25*, 355-368.

Smith, M.I., Yatsunenkov, T., Manary, M.J., Trehan, I., Mkakosya, R., Cheng, J., Kau, A.L., Rich, S.S., Concannon, P., Mychaleckyj, J.C., *et al.* (2013a). Gut microbiomes of Malawian twin pairs discordant for kwashiorkor. *Science* *339*, 548-554.

Smith, P.M., Howitt, M.R., Panikov, N., Michaud, M., Gallini, C.A., Bohlooly, Y.M., Glickman, J.N., and Garrett, W.S. (2013b). The microbial metabolites, short-chain fatty acids, regulate colonic Treg cell homeostasis. *Science* *341*, 569-573.

Tautenhahn, R., Cho, K., Uritboonthai, W., Zhu, Z.J., Patti, G.J., and Siuzdak, G. (2012). An accelerated workflow for untargeted metabolomics using the METLIN database. *Nature biotechnology* *30*, 826-828.

Tolhurst, G., Heffron, H., Lam, Y.S., Parker, H.E., Habib, A.M., Diakogiannaki, E., Cameron, J., Grosse, J., Reimann, F., and Gribble, F.M. (2012). Short-chain fatty acids stimulate glucagon-like peptide-1 secretion via the G-protein-coupled receptor FFAR2. *Diabetes* *61*, 364-371.

Tremaroli, V., and Backhed, F. (2012). Functional interactions between the gut microbiota and host metabolism. *Nature* *489*, 242-249.

Walker, A.W., Ince, J., Duncan, S.H., Webster, L.M., Holtrop, G., Ze, X.L., Brown, D., Stares, M.D., Scott, P., Bergerat, A., *et al.* (2011). Dominant and diet-responsive groups of bacteria within the human colonic microbiota. *ISME J* *5*, 220-230.

Wang, T.J., Larson, M.G., Vasan, R.S., Cheng, S., Rhee, E.P., McCabe, E., Lewis, G.D., Fox, C.S., Jacques, P.F., Fernandez, C., *et al.* (2011). Metabolite profiles and the risk of developing diabetes. *Nature medicine* *17*, 448-453.

Wishart, D.S., Jewison, T., Guo, A.C., Wilson, M., Knox, C., Liu, Y.F., Djoumbou, Y., Mandal, R., Aziat, F., Dong, E., *et al.* (2013). HMDB 3.0-The Human Metabolome Database in 2013. *Nucleic Acids Res* *41*, D801-D807.

Wu, G. (2009). Amino acids: metabolism, functions, and nutrition. *Amino acids* *37*, 1-17.

Wu, G.D., Chen, J., Hoffmann, C., Bittinger, K., Chen, Y.Y., Keilbaugh, S.A., Bewtra, M., Knights, D., Walters, W.A., Knight, R., *et al.* (2011). Linking long-term dietary patterns with gut microbial enterotypes. *Science* *334*, 105-108.

Wu, G.D., Compher, C., Chen, E.Z., Smith, S.A., Shah, R.D., Bittinger, K., Chehoud, C., Albenberg, L.G., Nessel, L., Gilroy, E., *et al.* (2014). Comparative metabolomics in vegans and omnivores reveal constraints on diet-dependent gut microbiota metabolite production. *Gut* *gutjnl-2014-308209*.

Ze, X.L., Duncan, S.H., Louis, P., and Flint, H.J. (2012). *Ruminococcus bromii* is a keystone species for the degradation of resistant starch in the human colon. *ISME J* *6*, 1535-1543.

Zeller, G., Tap, J., Voigt, A.Y., Sunagawa, S., Kultima, J.R., Costea, P.I., Amiot, A., Bohm, J., Brunetti, F., Habermann, N., *et al.* (2014). Potential of fecal microbiota for early-stage detection of colorectal cancer. *Molecular systems biology* *10*, 766.

Zomorodi, A.R., and Maranas, C.D. (2012). OptCom: a multi-level optimization framework for the metabolic modeling and analysis of microbial communities. *PLoS computational biology* *8*, e1002363.

FIGURE LEGENDS

Figure 1 Validation of the GEMs

- (a) Each GEM was validated based on the rRNA and metabolomics data generated by *in vitro* experiments. The byproducts and the substrate usage were constrained in the models and the growth rate was compared with the experimental data.
- (b) Predicted and measured SCFA levels by the individual bacteria. Propionate was produced only by *B. thetaiotaomicron*, while acetate was produced by Actinobacteria and Bacteroidetes phyla. Butyrate production was mainly produced by the bacteria from the class clostridia.
- (c) Predicted and measured biomass at the end of the fermentations. Growth was set as an objective function for each model and the predicted growth was compared with the experimental data.
- (d) Predicted and measured levels of AAs by the individual bacteria. Each model also predicted AA levels and the details of 15 significant amino acids produced are shown for each bacterium. The predicted and experimental values showed that all AAs could be produced in the range of experimental data with specific optimum solution. Data are presented as mean value \pm SD. See also Table S1 and S2 for more details.

Figure 2 Validation of the CASINO Toolbox

- (a) Two *in-silico* microbial communities EBBR (*E. rectale* + *B. adolescentis* + *B. thetaiotaomicron* + *R. bromii*) and FBBR (*F. prausnitzii* + *B. adolescentis* + *B. thetaiotaomicron* + *R. bromii*) were designed and simulated using the CASINO Toolbox. The results were compared with data from triplicate *in-vitro* experiments for EBBR and FBBR communities. In CASINO the interactions of the bacteria as well as the phenotype of the community were identified using an optimization algorithm. Growth of each bacterium had local optimum whereas the community had global optimum. The community optimum was detected by the intersection point of the fixed constraints for the community and the calculated dynamic constraints, which was obtained by summation of the local and community forces. See Figure S1 for development of the toolbox. See Table S3 for more details.
- (b) Predicted and measured levels of SCFA and AAs by the two *in-silico* microbial communities including EBBR (*E. rectale*, *B. adolescentis*, *B. thetaiotaomicron* and *R. bromii*) and FBBR (*F. prausnitzii*, *B. adolescentis*, *B. thetaiotaomicron* and *R. bromii*). We found that synthesis of essential AAs (histidine, isoleucine, leucine, lysine, methionine, phenylalanine, threonine and valine) produced by the communities is higher than the production of non-essential AAs (alanine, glutamate, glycine, proline, serine and tyrosine). Data are presented as mean value \pm SD. See Figure S2 for details of AAs prediction.

Figure 3 The network structure influence and sensitivity analysis on CASINO.

- (a) The community of *B. thetaiotaomicron*, *B. adolescentis*, *F. prausnitzii*, *E. rectale* and *R. bromii* were tested based on being receptor (receiving metabolites from the other microbes) or effector (producing metabolites where consumed by receptors). Two methods of centrality were tested on these networks (power centrality and degree

centrality). Calculated centrality scores determined *E.rectale* as the most important receptor and *B.thetaiotaomicron* as the most important effector.

- (b) The sensitivity of CASINO optimization was tested by evaluating the changes in SCFA profile upon adding different species to the community. First the most important receptor and effector in the communities were identified using the result of Figure 3A. 1 mmol/l of glucose was used for all the simulations and the SCFAs profile were predicted. Following identification of the dominant receptor and effector, the key species, the other species were added to the community one by one until the EBBR and FBBR community were reconstructed. Comparison between the simulations showed that the SCFA profile is very sensitive to the absence and existence of species with respect to their abundance and interactions.

Figure 4 The effect of the 6 weeks diet interventions in HGC and LGC individuals.

- (a) For each food source the major macronutrients were quantified and this enabled using the CASINO Toolbox to study the effect of the diet on the gut microbiota composition of subjects classified based on their microbial gene richness.
- (b) Abundance of species before and after diet interventions in HGC and LGC subjects. Data are shown as box-plots with *E. coli* (red), *B. thetaiotaomicron* (yellow), *B. adolescentis* (jade), *L. reuteri* (brown), *F. prausnitzii* (blue) and *E. rectale* (green). The heat map shows the p-values for four different comparisons of the species levels (each row associated with the corresponding species indicated in the left part of the figure). See Table S5 for more details.
- (c) A diet algorithm was developed and implemented for prediction of the macromolecules present in different food sources and this allowed further conversion of diets to three main categories of macronutrients carbohydrates, fiber and AAs. See table S6 and S7 for more details.

Figure 5 The effect of the 6 weeks diet interventions in predictions and fecal metabolomics of HGC and LGC individuals

- (a) Summary of average phenotypic predictions for baseline and after 6 weeks. The group of metabolites in the top right hand of the figure denotes the predictions at baseline and at the bottom left represents predictions after 6 week of dietary intervention. Subtracting the \log_{10} average metabolite fluxes for HGC from LGC is represented on the x-axis and the summation on the y-axis. The x-axis shows the ratio of predicted metabolite levels between HGC and LGC and the y-axis the sum of predicted metabolite levels in the two groups. The colors show the metabolites distance from zero in y-axis (from dark blue at the top to dark red at the bottom).
- (b) Metabolomics analysis of fecal samples obtained from HGC and LGC subjects. The differences are shown for 14 detected AAs as well as for butyrate.
- (c) p-values based on Student's t-test for specification of significantly changed metabolites for four different comparisons. B stands for baseline (before the dietary intervention), w6 stands for week 6 (after the dietary intervention).

Figure 6 The serum metabolomics validated the predictions and fecal metabolomics

- (a) Metabolomics of the serum samples obtained from HGC and LGC individuals. The 10 AAs and acetate were quantified at the baseline (b) and week 6 (w6).

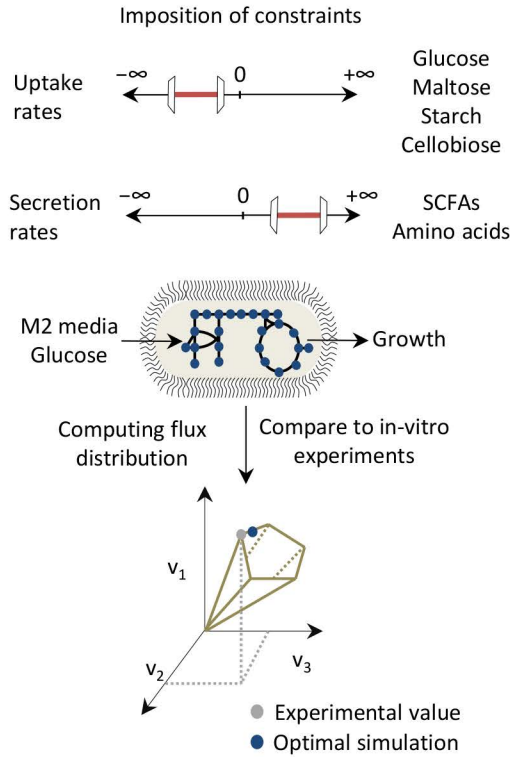
- (b) p-values based on Students t-test for specification of significantly changed metabolites between HGC and LGC at baseline and week 6.
- (c) Correlation of the 10 quantified AAs in serum with different clinical parameters of HGC and LGC subjects. The figure shows significant correlations ($p < 0.05$) with the color code specifying the slope of the correlation. Fat mass was measured by biphotonic absorptiometry (DXA). MIP1b: Macrophage inflammatory protein 1b; sCD14: soluble CD14; hsCRP: human sensitive CRP; HOMA-IR: Homeostatic model assessment-insulin resistance = $\frac{Glucose \times Insulin}{22.5}$ BMI: Body Mass Index (kg/m²); Disse index = $12 \times \left[2.5 \times \left(\frac{HDL}{Total\ Cholesterol} \right) - FFA \right] - Insulin$; MIP1b: Macrophage inflammatory protein 1b; sCD14: soluble CD14; hsCRP: human sensitive CRP; NEFA: non esterified fatty acids. See Table S4 for details of clinical parameters.

Figure 7 Modeling the dietary composition to transfer LGC individuals towards improved phenotype

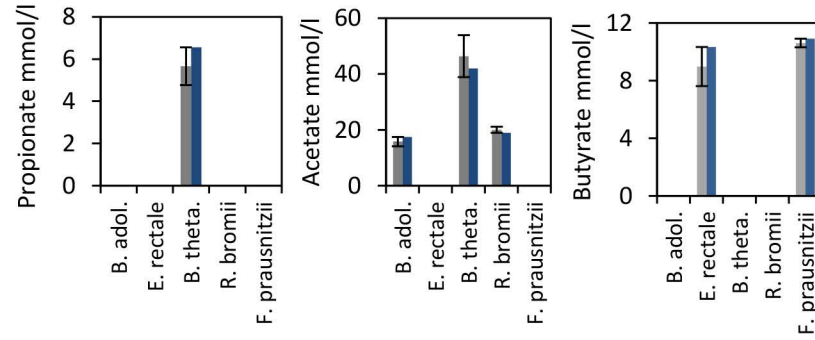
- (a) The yellow circles specify the simulated consumption of the 8 essential AAs by the gut microbiome of the LGC individuals at baseline (base phenotype) and the green circles specify the simulated consumption of the 8 essential AAs for the HGC individuals at week 6 (improved phenotype).
- (b) After calculating the required amount of 8 essential AAs at base and improved phenotype, both patterns were correlated with composition of AAs in different food categories. The direction of the $Corr_{Improved} - Corr_{Base}$ indicates the positive/negative effect of different food sources to improve the phenotype of LGC subjects. ($Corr_{Base}$: correlation between pattern AAs in base phenotype and food, $Corr_{Improved}$: correlation between pattern AAs in improved phenotype and food). See Table S8 for more details.

Figure 1

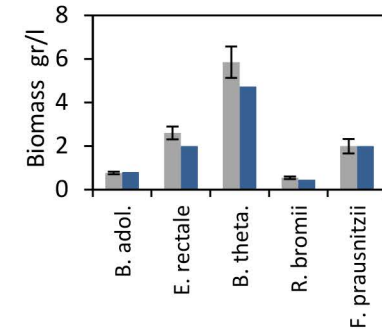
A



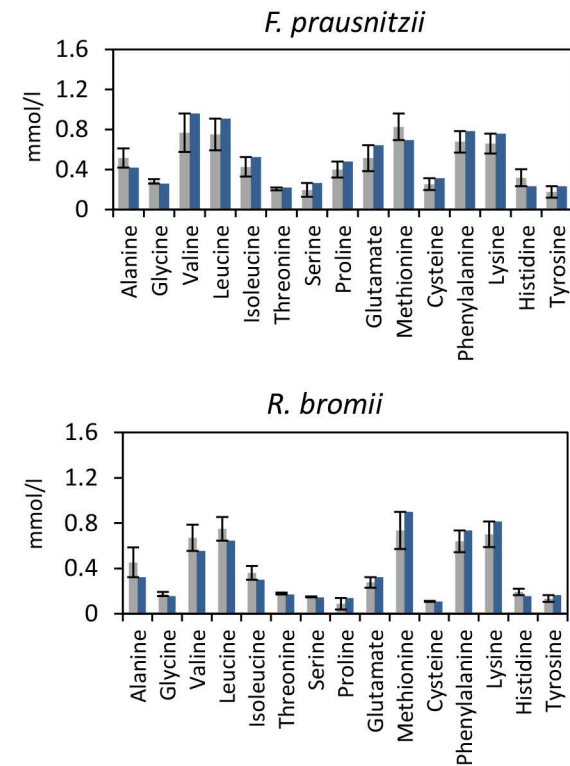
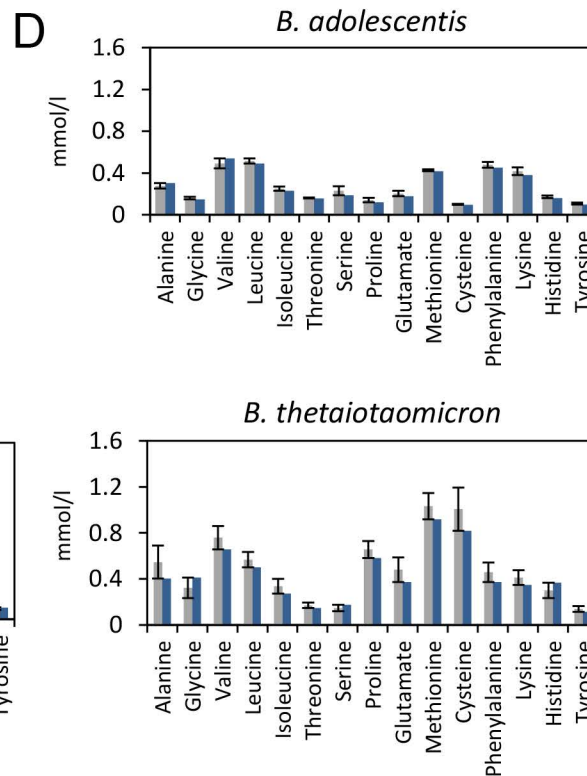
B



C



D



Simulation ■
 Experimental ■

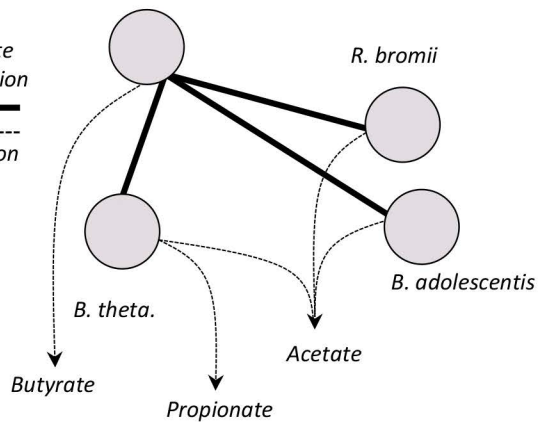
Figure 2

A

EBBR/FBBR

E. Rectale / *F. prausnitzii*

Acetate Interaction
 ——— Secretion

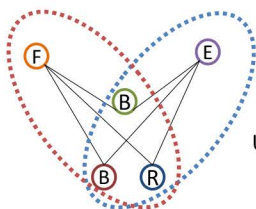


EBBR (M2 + Starch + Cellobiose)

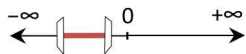
FBBR (M2 + Starch + Cellobiose)

Genomics
& metabolomics

Imposition
of constraints



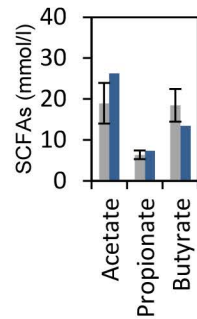
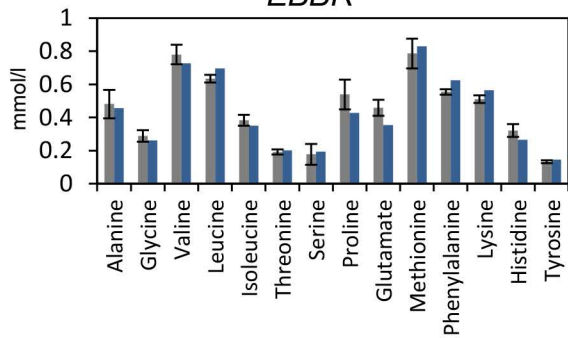
Uptake rates



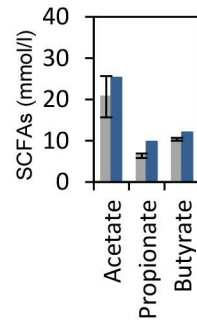
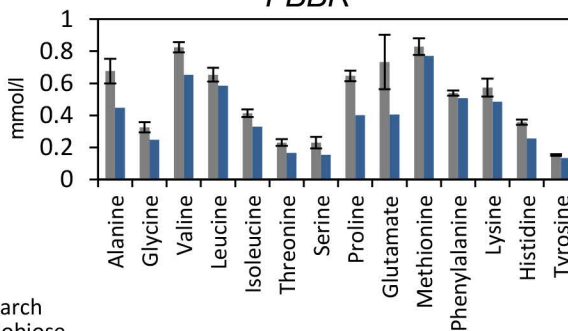
Starch
Cellobiose

B

EBBR



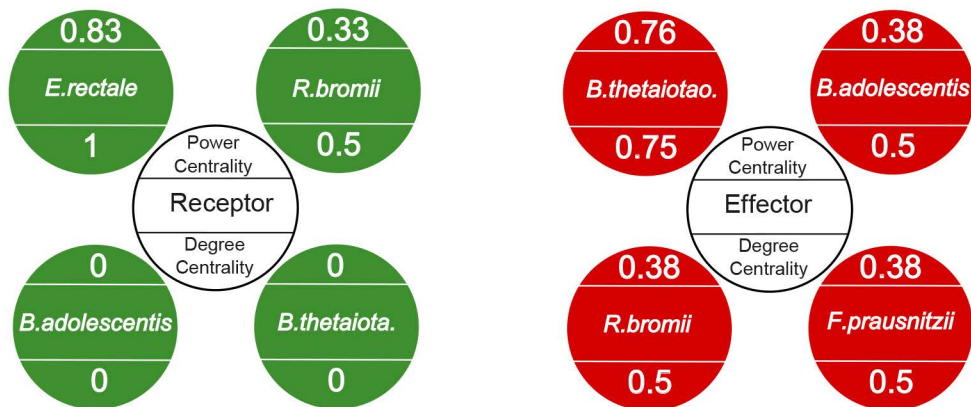
FBBR



Simulation ■
 Experimental ■

Figure 3

A



B

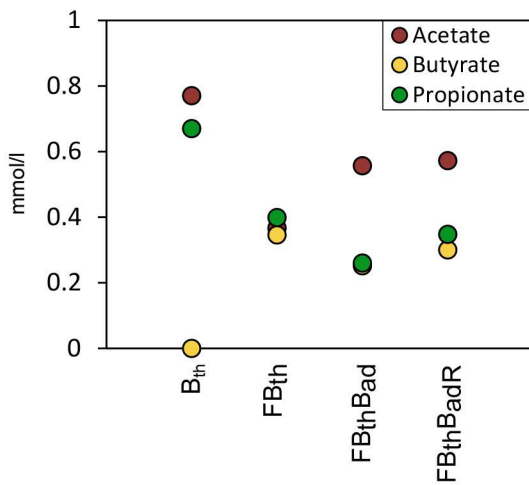
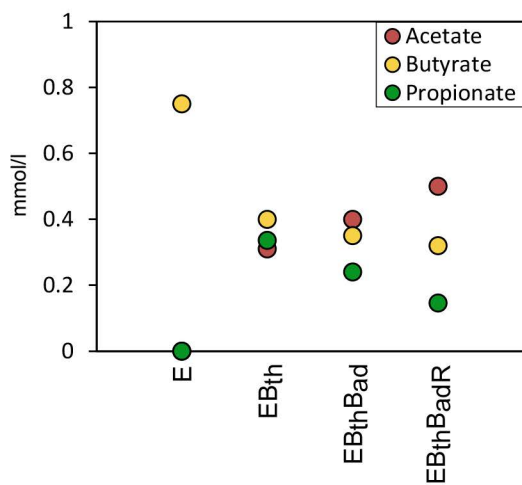
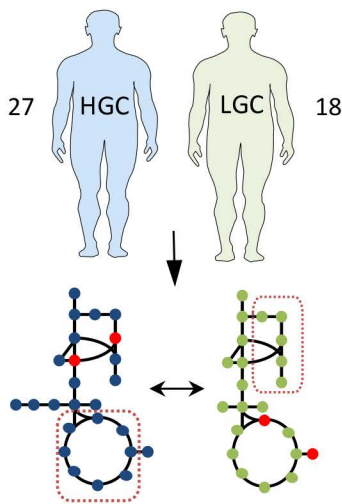
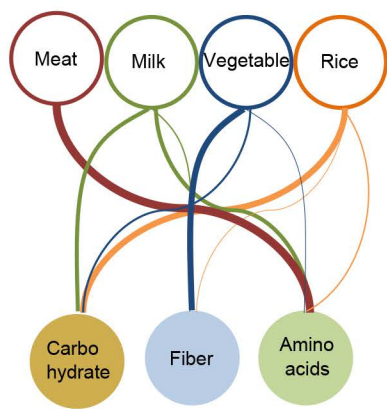
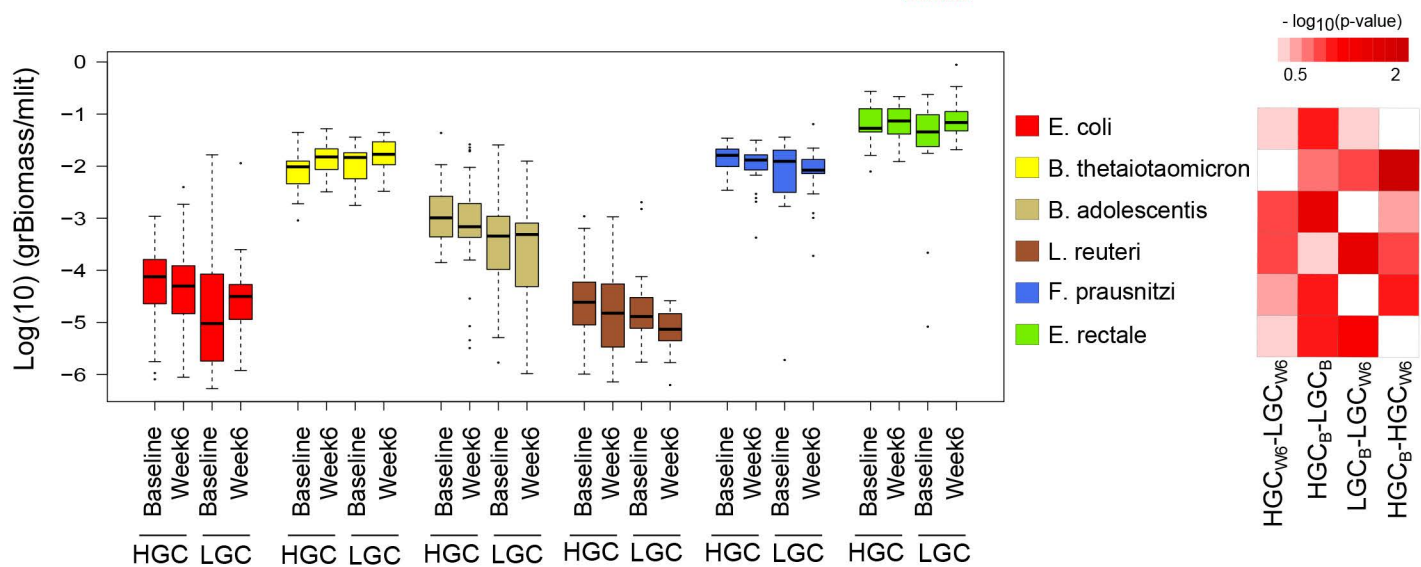


Figure 4

A



B



C

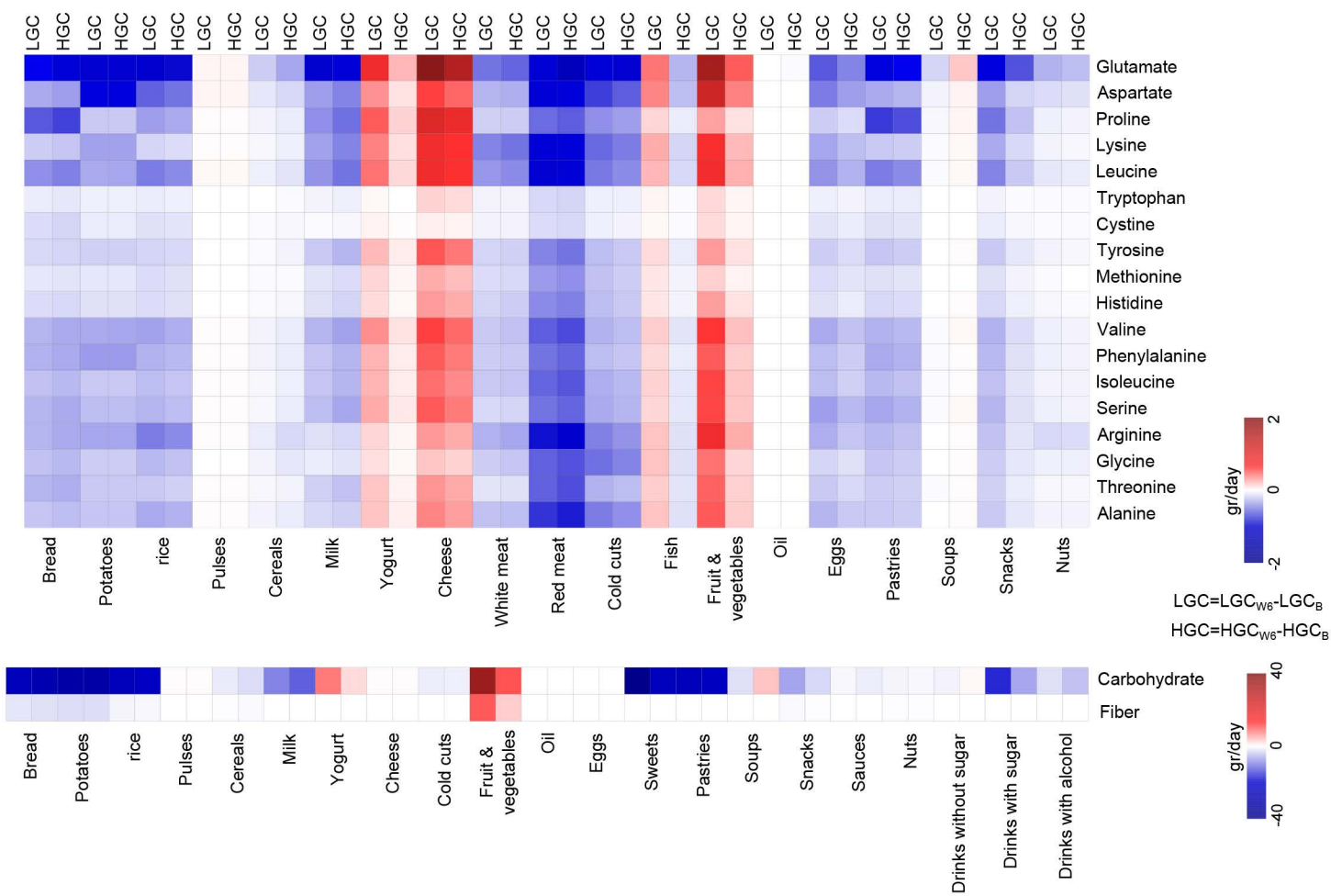


Figure 5

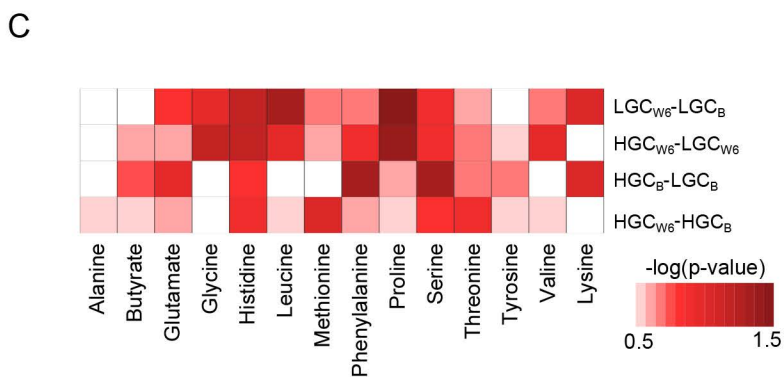
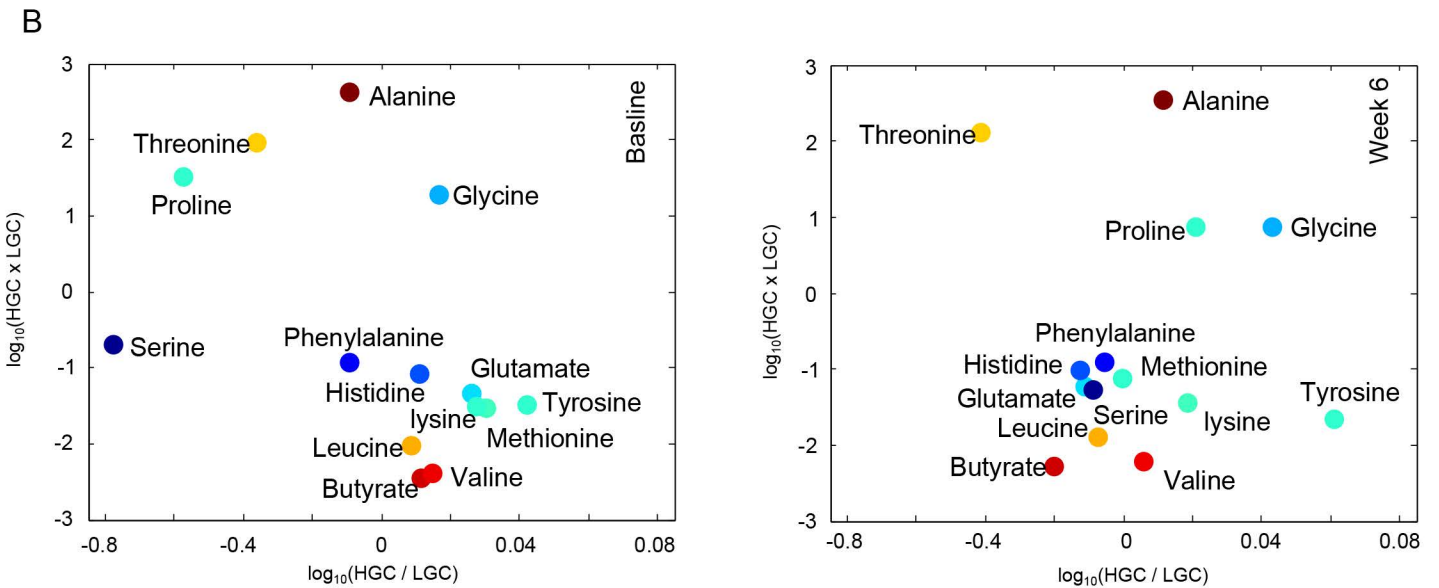
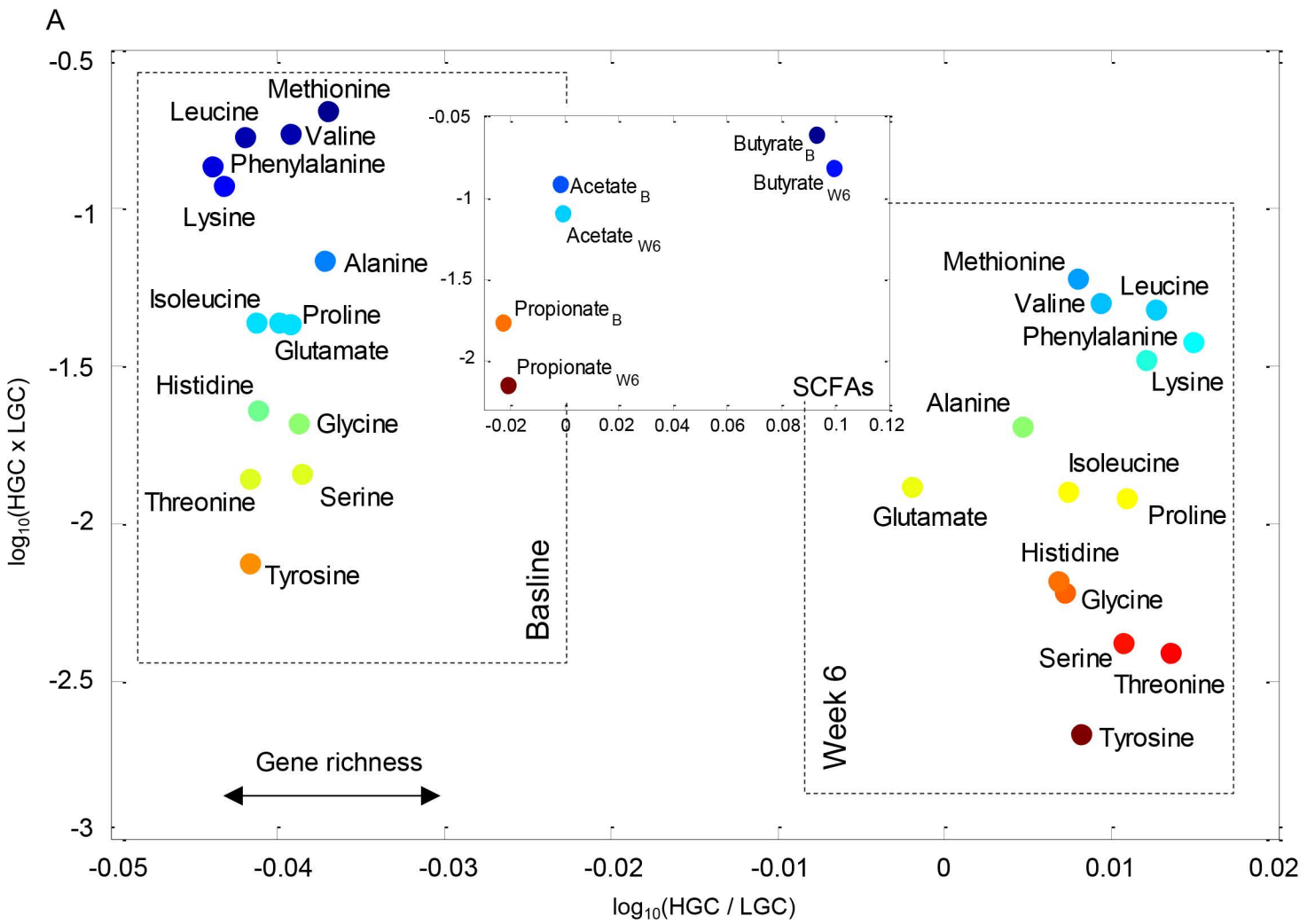


Figure 7

